IVUS IMAGE AUTOMATIC SEGMENTATION USING A HOPFIELD NEURAL NETWORK AND 3D RECONSTRUCTION OF STENOTIC ARTERIAL SEGMENTS

M.E. Plissiti, D.I. Fotiadis and L.K. Michalis

33 – 2001

Preprint, no 33 – 01 / 2001

Department of Computer Science
University of Ioannina
45110 Ioannina, Greece

IVUS Image Automatic Segmentation Using a Hopfield Neural Network and 3D Reconstruction of Stenotic Arterial Segments

M. E. Plissiti[(1)], D. I. Fotiadis[(1)] and L. K. Michalis[(2)]

[(1)] Dept. of Computer Science, University of Ioannina, 45110 Ioannina, Greece

[(2)] Dept. of Cardiology, Medical School, University of Ioannina, 45110 Ioannina, Greece

Abstract

In this paper we present a method, which includes automated detection of regions of interest in sequential Intravascular Ultrasound (IVUS) frames and combination of the extracted results with biplane angiography data. The application of the proposed method in the entire IVUS image sequence, in combination with the processing of two perpendicular angiographic images, produces a three dimensional model of the examined arterial segment, where the stenotic areas are depicted in detail. The detection of regions of interest is performed using deformable models. The energy function is appropriately modified and is minimized using a Hopfield neural network. The method includes boundary correction schemas, which introduce suitable initial estimations for sequential frames. The 3D reconstruction is based on the computation of the pullback path and appropriate placement of the detected boundary points. The method is used in several cases and the obtained results are illustrated.

Key Words: IVUS segmentation; 3D artery reconstruction.

I. INTRODUCTION

Atherosclerosis is the disease that causes partial or total obstruction of human arteries. The infection of coronary arterial segments by this disease requires early diagnosis and accurate assessment of plaque 3D geometry for the selection of the appropriate therapeutic method. Several imaging techniques exist for the estimation of the severity of the disease *in vivo*. Intravascular ultrasound (IVUS) and biplane coronary angiography are commonly used diagnostic tools. The first permits direct visualization of the arterial wall morphology, while the second produces accurate information about the lumen as well as the vessel topology and shape.

IVUS requires insertion of a catheter in the vessel. A small transducer is placed at the tip of the catheter, which transmits a high-frequency (20-40 MHz) ultrasound signal. The attenuation of the signal, while passing through the vessel and its adjacent tissues generates cross-sectional images. An image sequence is acquired during the constant speed catheter's pullback along the vessel. In those images the region of the lumen and the outer layers of the vessel can be identified and the percentage of stenosis can be calculated. Furthermore, plaque characteristics are obvious in many cases and typical plaque components, such as calcium, can be detected.

IVUS exhibits certain advantages such as real time visualization of plaque morphology, quantification of plaque eccentricity and detection of lumen borders for the assessment of wall thickness. However, IVUS does not provide information regarding vessel topology or its location in the 3D space. This information, which is needed for the specification of stenotic areas along the vessel, can be derived by biplane angiography. Using biplane angiography, two images of the arterial lumen are produced from different projection rays and the vessel curvature can be extracted by processing those images.

A lot of effort has been made to combine the information extracted from these techniques in order to reconstruct accurately the arterial segment [1, 2, 3, 4]. Several techniques have been proposed concerning the automated detection of the regions of interest in individual IVUS frames and afterwards the 3D reconstruction of the arterial lumen. These techniques can be classified depending on the information they use and the methods they apply in image segmentation for the detection of the wall borders.

The techniques for automated identification of the regions of interest in IVUS frames take advantage of the characteristic appearance of the arterial anatomy in two dimensional IVUS images. Some of the earlier work on segmentation of IVUS images was based on graph searching algorithms. The cost function, which was used in the border detection process, incorporated *a priori* information of the expected pattern in IVUS frames [5, 6]. Also, in this direction, segmentation methods based on probabilistic approaches have been proposed [7, 8]. A class of methods that take advantage of the expected similarity of the regions of interest in adjacent IVUS frames takes into account that the sequence of frames constitute a three dimensional object. On this object, active contour principles [9, 10] or boundary detection in 3D space [11] can be used to extract the desired contours of lumen and vessel. Other methods use the information from two perpendicular longitudinal sections from the entire 3D object to detect lumen borders [12, 13]. Afterwards, they combine this result with the corresponding planar images, to extract the final contour.

In order to generate a 3D model of the arterial segment, several approaches have been proposed. Methods that are based only on the information extracted from biplane angiography for the 3D reconstruction of arterial segments [14, 15] are restricted by the loss of the lumen width, because the three dimensional object (lumen) is projected on a plane. Furthermore, methods that make the assumption that IVUS frames are parallel to each other [9, 16] and the 3D transducer pullback trajectory is approximated by a straight line, comprise a volume error due to its under or overestimation in curved vessel segments [17].

To avoid these drawbacks, fusion of biplane angiography and IVUS images is performed to result in a reliable model of the artery. The lumen's border is obtained by the processing of IVUS images and the curvature of the vessel is extracted from biplane angiography [2, 3, 4]. For the determination of the curvature, the catheter's path in angiographic images is required. In this direction, two approaches are used, depending on the information contained in angiographic images: estimation of the catheter's path using the vessel centerline [2] or extraction of the catheter's path in the lumen, when this is visible [18, 3]. The last step in the 3D reconstruction process is the mapping the IVUS images to their location on the catheter's path.

In this work, we focus on the development of a fast and automated method for accurate IVUS image segmentation and the 3D reconstruction of the arterial segment. User interaction is required only in the first frame of the sequence, for setting an initial estimation for the border of the lumen and the boundary between media/advenitia. A robust method, based on deformable models, is applied sequentially on the entire set of IVUS frames for the extraction

of the borders of region of interest. The modification of the energy function of the deformable model makes the use of a Hopfield neural network feasible for the minimization of the energy function, which results in the reduction of the processing time for each frame. Furthermore, the introduction of a new expression for the image energy makes the method stable resulting in accurate boundaries for all images, regardless of the presence of noise or weak edges, both common in IVUS imaging. In each frame, a smooth initial deformable curve is provided by the computation of the convex hull of the extracted boundary in the previous frame. The method is applied twice in each frame. The outcome of the first application is the boundary between media/adventitia and is used for the restriction of the searching space for the determination of the lumen border. The extracted curves from the entire IVUS sequence are placed in 3D space to obtain a 3D model of the arterial segment. The curvature of the vessel is estimated with the use of two perpendicular angiographic images. The three dimensional representation of the artery segment is obtained through a 3D reconstruction method.

II. METHODS

A. IVUS Image Segmentation Method

The extraction of the regions of interest in individual IVUS frames is performed by a method based on the basic principles of deformable models, which takes advantage of the knowledge of the quality of a single image and use it to find the corresponding regions in sequential frames. The initial estimation for the searching area is provided by the previously processed frame. The use of the Hopfield neural network for energy minimization makes the method fast.

Preprocessing

IVUS frames contain noise and the actual boundaries of regions of interest are difficult to be identified in many cases. Image preprocessing removes speckles and artifacts that can interfere with the detection of desired boundaries, during the selection process. Furthermore, the detection of regions of interest is restricted by the weak edges in IVUS images and image enhancement is required. We use a 3×3 median filter to eliminate the effect of speckles, without blurring the edges. A band-pass linear filter is then applied for the sharpening of image edges whose thresholds are determined empirically.

Boundaries Detection

1. Initial Estimation

The regions of interest in IVUS images are detected automatically in the entire frame sequence. The borders of lumen/intima and media/adventitia, which delimit the region of plaque in the arterial wall must be extracted. The method is applied twice in each IVUS frame, with some modifications, for the detection of both boundaries. Since our approach is based on deformable models, an initial contour for the lumen/intima and media/adventitia boundary must be provided. The initial estimation of the region of interest must be in proximity to the real boundary, otherwise the deformable model does not converge. The observer, interactively, gives a set of points on the estimated boundary, and a closed curve is produced drawing line segments between those points (Fig. 1). The number of sampled points is not constant and depends on the smoothness of the region. Regions of interest that are not ellipse-like shaped may require more points to be defined accurately.

The catheter is moving into the vessel with a constant speed of 1 mm/sec. Given that the frame storage rate is about 25 frames/sec, contours in adjacent frames must have similar shape. Thus, we use the contour detected in the current frame as the initial estimation for the next frame. This process is applied on the entire image IVUS sequence.

2. Active Contour Model

The initial estimation of the boundary of the region of interest forms an active curve, which deforms in order to obtain the final shape of the actual boundary. As proposed in [19], a snake deforms with the influence of internal and external forces and is attracted to image characteristics. The position of the snake is represented parametrically as $v(s) = (x(s), y(s))$, and the corresponding energy functional is:

$$E_{\text{snake}} = \int_0^1 \left(E_{\text{int}}(v(s)) + E_{\text{image}}(v(s)) \right) ds, \tag{1}$$

where E_{int} represents the internal energy of the snake due to bending and E_{image} is derived from image data. As in most conventional snake models, the internal energy is a function of the first and second order derivatives of the curve, and is expressed as:

$$E_{\text{int}} = \alpha(s)|v'(s)|^2 + \beta(s)|v''(s)|^2. \tag{2}$$

E_{image} is the term that forces the snake to be attracted to image features, and is defined as:

$$E_{\text{image}} = -\gamma(s)|\nabla I|^2, \tag{3}$$

where $|\nabla I|$ is the image gradient, and $\alpha(s)$, $\beta(s)$ and $\gamma(s)$ are the elastic factors.

In the discrete domain, the first and second order derivatives of the snake can be approximated by a finite difference scheme, and assuming constant elastic factors, the energy function of the snake can be expressed as:

$$E_{\text{snake}} = \sum_{i=1}^{N} \left\{ \alpha (v_i - v_{i-1})^2 + \beta (v_{i-1} - 2v_i + v_{i+1})^2 - \gamma g_i \right\}$$

$$= \sum_{i=1}^{N} \left\{ \alpha \left[(x_i - x_{i-1})^2 + (y_i - y_{i-1})^2 \right] + \beta \left[(x_{i-1} - 2x_i + x_{i+1})^2 + (y_{i-1} - 2y_i + y_{i+1})^2 \right] - \gamma g_i \right\}, \quad (4)$$

where N is the number of points of the snake and g_i is the image gradient at each image pixel. The pixels of the image that minimize this energy function and are close to the region of interest define the boundaries of the desired region. The energy of the snake is minimized, with the use of a Hopfield neural network, which reduces the searching time needed for the selection of the appropriate image pixels.

3. *Application of the Hopfield Neural Network*

A typical Hopfield neural network [20] consists of a single layer of neurons, where each neuron has one of the two outputs, $o = 0$ or $o = 1$ (firing or not firing). A Hopfield network is fully interconnected with no specific input or output layer. Each node has a bias I and is connected with every other node. The connections are bi-directional and symmetric and a specific weight T_{ij} is assigned to each connection. The state u of each neuron depends on the input it receives from other neurons, and is given as:

$$u_i = \sum_{j \neq i}^{N} T_{ij} o_j + I_i, \quad (5)$$

where N is the number of neurons. The total energy function of the network can be expressed as:

$$E = -\frac{1}{2} \sum_{i=1}^{N} \sum_{j=1}^{N} T_{ij} o_i o_j - \sum_{i=1}^{N} I_i o_i . \quad (6)$$

The network converges when the energy function reaches a local minimum.

The energy of a deformable curve can be minimized using a Hopfield neural network [21]. The nodes of this network correspond to image pixels and the pixels that minimize the total energy of the network form the desired boundary. The network consists of one layer of $N \times M$ neurons (Fig. 2). Given the initial estimation curve, N points were sampled and

perpendicular line segments consisted of M points are drawn. Each neuron (i, j), $1 \le i \le N$, $1 \le j \le M$, represents a candidate point of the final boundary. The output of the neuron is zero, for a point that is not included in the set of the boundary points, and one, for a point that belongs to the boundary set.

The energy of the snake which will be minimized by a Hopfield neural network, can be expressed as:

$$E = \sum_{i=1}^{N} \left\{ \begin{array}{l} \alpha \left[\left(\sum_{k=1}^{M} x_{ik} o_{ik} - \sum_{k=1}^{M} x_{i-1k} o_{i-1k} \right)^2 + \left(\sum_{k=1}^{M} y_{ik} o_{ik} - \sum_{k=1}^{M} y_{i-1k} o_{i-1k} \right)^2 \right] + \\ \beta \left[\begin{array}{l} \left(\sum_{k=1}^{M} x_{i-1k} o_{i-1k} - 2 \sum_{k=1}^{M} x_{ik} o_{ik} + \sum_{k=1}^{M} x_{i+1k} o_{i+1k} \right)^2 + \\ \left(\sum_{k=1}^{M} y_{i-1k} o_{i-1k} - 2 \sum_{k=1}^{M} y_{ik} o_{ik} + \sum_{k=1}^{M} y_{i+1k} o_{i+1k} \right)^2 \end{array} \right] - \\ \gamma \left[\sum_{k=1}^{M} g_{ik} o_{ik} \right] \end{array} \right\}, \quad (7)$$

where x, y are the coordinates of a point, o is the output of a neuron, and g is the image energy.

The interconnective strengths are given as:

$$T_{ikjl} = -\left[\begin{array}{l} (4\alpha + 12\beta)\delta_{ij} - (2\alpha + 8\beta)\delta_{i+j} - (2\alpha + 8\beta)\delta_{i-j} \\ + 2\beta\delta_{i+2j} + 2\beta\delta_{i-2j} \end{array} \right] \left[x_{ik} x_{jl} + y_{ik} y_{jl} \right], \quad (8)$$

where

$$\delta_{ij} = \begin{cases} 1, if \ i = j \\ 0, \text{otherwise} \end{cases}, \quad (9)$$

and the bias for each neuron is $I_{ik} = \gamma g_{ik}$.

At every iteration the state of each neuron (i, k) is updated according to:

$$u_{ik} = \sum_{j=1}^{N} \sum_{l=1}^{M} T_{ikjl} o_{jl} + I_{ik}. \quad (10)$$

The output of the neuron is determined by the function: $o_{ik} = f(u_{ik})$, where:

$$f(u_{ik}) = \begin{cases} 1, if \ u_{ik} = \max(u_{ih}; h = 1,2,...M) \\ 0, \text{otherwise} \end{cases}. \quad (11)$$

Using relations (5) – (11) we can initialize the strengths for each connection, the state, output and bias for each neuron, and finally, the total energy of the network. In the first iteration, the output of all neurons is zero, except those neurons that correspond to points of the initial estimation contour.

After the construction of the network an iterative procedure is followed described by the following steps:

- Update the state of each neuron synchronously.
- If the new state of the neuron reduces the total energy of the network, then the new state is acceptable and the states of all neurons and the total energy of the network are updated, otherwise no state change is affected.
- Check the total energy of the network. If the energy does not change anymore, the network has reached a local minimum of the function.
- The firing neurons form the new boundary for the region of interest.

4. *Specification of the Searching Grid*

An important step of the segmentation algorithm is the definition of the area where the initial contour can deform to equilibrate to the final contour. The searching area consists of line segments that are perpendicular to the initial contour, at some sampled points. The sampling process of the initial contour requires the calculation of the center of the contour points, which is given by:

$$\mu_j = \left(\overline{x}_j, \overline{y}_j\right) = \frac{1}{n_j} \sum_{i=1}^{n_j} \left(x_{ij}, y_{ij}\right), \tag{12}$$

where j is the number of the contour, containing n_j points with coordinates (x_{ij}, y_{ij}). μ_j is considered to be the center of the ellipse-like curve, from which we draw two perpendicular lines that intersect the contour at four points and divide it into four separate regions. Starting from every one of these four points, we move anti-clockwise and at equal angles of 15° we sample five points at every region. The total number of the sampled points at each contour is 24, which is sufficient to reach a smooth final contour. Then, perpendicular line segments are drawn centered at sampled points. The number of points included in each segment is different for the inner and outer boundary. These points are the candidate points for the final contour and one point of each line segment will be selected as a point of the final contour.

5. *Proposed Image Energy*

The intensity or the gradient of the image at specific pixels is included in the image energy expression. For the detection of strong edges it is essential to push the snake to contours which correspond to large image gradients. In general, the gradient of the image is computed using standard operators for row and column gradient. A limitation common to all edge gradient operators is their inability to accurately detect edges in high noisy environments such as IVUS images. In these images, the distribution of the pixels, which correspond to regions of specific tissues, is not homogenous and their intensity varies in a small range. Furthermore, pixels with large image gradient may appear due to noise speckles introduced from the ultrasound signal. These pixels do not indicate the real border of the region, but they attract the snake towards their position, which may entail wrong identification of the boundary of the region of interest. For this reason, we try to find those edges that separate large regions with small intensity variations in IVUS images.

For the detection of the actual boundary of the region of interest we calculate the mean intensity value of four adjacent areas of fixed size at a specific pixel (Fig 3). The size of those areas depends on the boundary of the region we are interested in, for example the lumen or the outer border of the vessel. For each pixel (i, j) the image gradient g_{ij} is defined as:

$$g_{ij} = \sqrt{\left(\overline{w}_u(i,j) - \overline{w}_b(i,j)\right)^2 + \left(\overline{w}_l(i,j) - \overline{w}_r(i,j)\right)^2}\,, \tag{13}$$

where $\overline{w}_u(i,j)$, $\overline{w}_b(i,j)$, $\overline{w}_l(i,j)$ and $\overline{w}_r(i,j)$ represent the mean values of the upper, lower, left and right windows of the pixel (i, j), respectively, computed as:

$$\overline{w} = \frac{1}{h^2} \sum_{k=-h/2}^{h/2} \sum_{l=-h/2}^{h/2} f(i+k, j+l)\,. \tag{14}$$

The size of noise speckles is normally small, compared to the region of the lumen or the media in IVUS images, so they do not affect the mean value of the intensity of the entire area. As a result, the snake is attracted by the pixels of the actual boundary of the region of interest and noise effects are suppressed. Fig. 4 illustrates the use of our approach with the new image energy term incorporated in the energy function of the deformable model, compared with the use of conventional image gradient operators, for the expression of the image energy.

6. *Convex Hull Calculation*

Small distortions in the shape of the final contour may cause abnormalities in the specification of the searching area for the next frame and there is a great probability of false detection of the wanted boundaries. The error introduced by non-convex initial estimation for the detection of the border between the media and adventitia is propagated in sequential

applications of the algorithm in several frames (Fig. 5(b)). For this reason, we look for smooth initial estimations for the boundary of media/adventitia.

In our method, the points extracted from the convergence of the network form a closed curve, which is the boundary of the region of interest. The shape of a cross sectional boundary of the border between media and adventitia is convex, according to the physiology of a healthy artery. This is also acceptable in the case where plaque appears in the vessel's wall, with the exception of highly diseased vessels, in which the morphology of the plaque is very complicated. For the definition of the final curve, which is used as the initial estimation of the border in the next frame, we calculate the convex hull of the final points (Fig. 6). The algorithm we have used is incremental and is related to plane sweep [22]. The convex hull is calculated only for the detection of the outer boundary of the vessel, while the shape of the border of the lumen can be more complicated and the approximation of the desired boundary with a convex curve may cause loss of information. As it is shown in Fig. 5 the need for the calculation of the convex hull is obvious in order to obtain an initial good estimation for the next frame.

7. Further Restrictions

The image segmentation method is applied twice on the entire sequence of IVUS frames (Fig. 7). The first application results in the detection of the border between media and adventitia, while the second concerns the detection of the boundary of the lumen. The outcome of the first application is stored and it imposes further limitations for the searching space of the inner boundary. On this way points of the searching lines that lay in the outer region of the vessel are not selected, during the iterative use of the neural network.

B. Three Dimensional Reconstruction of the Arterial Segment

A reliable three-dimensional representation of the arterial segment is essential for the accurate calculation of the characteristics related to the severity of the disease, such as the diameter and the length of the stenotic area and its exact position. Although IVUS images depict with detail the morphology of the plaque, they do not provide any information about the vessel topology or the location of each frame along the vessel. To produce a 3D model of the arterial segment, we need an estimation of the pullback path in 3D space, which is derived from the processing of angiographic data (Fig. 8). The extraction of the pullback path requires the processing of two angiographic images, acquired from two different projection views. The path is approximated with the vessel centerline in both images (Fig. 9) and it can be

reconstructed in 3D space. After the estimation of the 3D coordinates of the centerline, each IVUS frame is assigned to a specific location along the pullback path using its timestamp. Finally, the relative orientation for each IVUS frame is determined and each contour point is mapped in a plane perpendicular to the reconstructed 3D lumen centerline. The lumen centroids in IVUS frames coincide with the points in the centerline.

Angiographic Image Processing

Two angiographic images are obtained simultaneously with the IVUS examination. In those images adjacent tissues and bifurcations of the main vessel can be used as landmarks for the appropriate correspondence of the frames along the vessel path. For each angiographic image scale factors are calculated and each image was restored properly. Next the lumen borders are identified and the pullback path is approximated by the vessel centerline.

We use two perpendicular angiographic images to determine the xz and yz planes of an orthogonal system. The starting pullback point for both images coincides with the orthogonal system origin. The pullback path can then be reconstructed in 3D space from its known projections in both angiographic images. A curve is obtained from the set of points extracted, using linear interpolation, and is smoothed with the use of a 5-point averaging filter. The curve is then sampled uniformly; the number of sampled points corresponds to the number of frames of the IVUS sequence and each point represents the center of the lumen in 3D space. We assume that the transducer moves parallel to the vessel wall and the produced cross sectional images are perpendicular to the catheter's path.

Next we compute the plane which is perpendicular to the pullback path that corresponds to a specific frame. Initially, the IVUS frames are placed in planes that are parallel to each other and perpendicular to the z-axis of the orthogonal system. For the localization of the frames along z-axis, the timestamp of each frame is used, beginning from the first frame that corresponds to the pullback starting point. The distance between two sequential frames is unit. The center of the lumen at each frame is a point on the z-axis and the coordinates of the points that form the boundaries of the regions of interest are computed with the appropriate transformation. Given that the coordinates of the center μ of the lumen are (x_μ, y_μ) in the i-th frame, the new coordinates (x_p, y_p) for a point p of the boundary are computed as:

$$x'_p = x_p - x_\mu$$
$$y'_p = y_p - y_\mu \,. \qquad (15)$$
$$z'_p = i$$

The coordinates of the points of the boundary between media/adventitia are calculated in a similar manner.

The method includes transformation and translation of the points at a different orthogonal system that depends on the computed pullback path (Fig. 10). The idea is to determine a new reference system along the points of the path and to define the corresponding points of the boundaries in the new system. If the set of the points of the path in 3D space is $Q(q_1, q_2, ..., q_n)$ then every point of the frame i is translated in a way that the new center of the lumen will be the point q_i.

The determination of the new orthogonal system requires the calculation of the direction cosines of the new axes. Given that the IVUS frames are perpendicular to the catheter's path, the z′ axis is determined by the vector $q_{i+1} - q_i$. For the determination of x′ and y′ axes three sequential points q_i, q_{i+1}, q_{i+2} of the 3D catheter's path are considered. Those points define a plane and the vector product $\tau = \tau_1 \times \tau_2$, where $\tau_1 = q_{i+1} - q_i$ and, $\tau_2 = q_{i+2} - q_{i+1}$ is perpendicular to z′ axis and corresponds to the x′ axis. To define the conventional direction of the vector x′ (Fig. 11), we consider that the ordered set (τ_1, τ_2, τ) is a right-hand system. Thus, if the vectors τ_1 and τ_2 form a right turn, we calculate the vector product $\tau_1 \times \tau_2$, otherwise we take the opposite vector product. The vector's turn is calculated from the projection of the path in a plane where the torsion of the curve is not considered. In this plane, we have to check if the three points are collinear or coincide.

The new axis y′ is calculated from the vector product $x' \times z'$. To place the points of each frame in the new orthogonal system, it is essential to calculate the direction cosines of each axis. After the definition of the new orthogonal system, we consider the points $P_1(x_1, y_1, z_1)$, $P_2(x_2, y_2, z_2)$ and $P_3(x_3, y_3, z_3)$ on the axes x′, y′and z′, respectively. Given that the point $P_0(x_0, y_0, z_0)$ is the origin of the system, the direction cosines are defined as:

$$l_x = \frac{x_1 - x_o}{d_1}, \; m_x = \frac{y_1 - y_o}{d_1}, \; n_x = \frac{z_1 - z_o}{d_1}, \qquad (16a)$$

$$l_y = \frac{x_2 - x_o}{d_2},\ m_y = \frac{y_2 - y_o}{d_2},\ n_y = \frac{z_2 - z_o}{d_2}, \tag{16b}$$

$$l_z = \frac{x_3 - x_o}{d_3},\ m_z = \frac{y_3 - y_o}{d_3},\ n_z = \frac{z_3 - z_o}{d_3}, \tag{16c}$$

where d_i is the distance between P_i and P_0.

The coordinates of the points of the boundaries are given as:

$$\begin{bmatrix} x_p \\ y_p \\ z_p \end{bmatrix} = \begin{bmatrix} l_x & l_y & l_z \\ m_x & m_y & m_z \\ n_x & n_y & n_z \end{bmatrix} \begin{bmatrix} x'_p \\ y'_p \\ z'_p \end{bmatrix} + \begin{bmatrix} q_x \\ q_y \\ q_z \end{bmatrix}. \tag{17}$$

The determined coordinates of the points of the boundaries produce a three dimensional grid of the arterial segment (Fig. 12).

III. RESULTS AND DISCUSSION

Sequences of IVUS images were used to test the image segmentation algorithm and two perpendicular angiograpphic images of the vessel were used for the reconstruction of the 3D geometry of the arterial segment. The initial estimation of the boundaries was given manually for the first frame.

The proposed approach is based on deformable models for the detection of both the boundaries of lumen and media/adventitia. Compared with conventional boundary-detection algorithms, snakes involve the incorporation of *a priori* knowledge, provided by the user. The estimation of the boundary is necessary before the application of the method in sequential frames. In our method the detected boundary is used as initial estimation for the next frame. The results of the method are not acceptable when the estimation is not good enough. We addressed two problems. The first is related with the modification of the image energy, since the use of conventional edge gradient operators results in highly distorted detected boundaries, due to the presence of noise in IVUS frames. The new term for image energy, introduced in the proposed method, results in the selection of pixels that belong to edges separating large and homogenous regions in the image. This is based on the fact that the areas of noisy pixels are small and they do not greatly influence the mean value of the intensity in large areas. The second is related to the computation of convex hull, which provides better and smoother boundary identification.

The determination of values of the parameters α, β, γ of the deformable model has been also addressed. The selection of the most suitable values was based on what each term denotes

physically. The first derivative in the internal energy determines the total length of the snake, while the second derivative controls the bending of the curve. Changing the values of the weights of the snake's terms will change the contribution of each term. We want the snake to be attracted mainly from the characteristics of the image and finally to have a smooth shape. After repeated applications of the method in several sequences of IVUS images, the values that yield acceptable results for the inner and outer boundary were $\alpha = 0.2, \beta = 0.1$ and $\gamma = 0.9$.

The use of the Hopfield neural network for the minimization of the snake's energy makes the application of the method in individual frames faster and computationally more efficient. The uniform separation of the searching domain in similar areas reduces the searching space and it takes advantage of the information contained in the entire neighborhood of the region of interest. The calculation of the convex hull produces smooth curves and ensures that the searching lines, which are formed at the next frame, will not coincide or will not be restricted in a small area, resulting in loss of significant image characteristics.

The application of the method yields accurate results, even if calcium appears in the media. In these cases, the border between media and adventitia is difficult to be detected, because of the dark shadow that calcium produces in the IVUS images. The detection of the borders of interest, when it is done manually, is an approximation of the real borders, and it is based on former images, where the actual borders are clear. The same is assumed in our method since the initial estimation of the region of interest depends on previous frames.

As far as 3D reconstruction is concerned, the proposed method is applicable in cases where the projection of the catheter in angiographic images is not visible. This is an important aspect, given that the angiographic images are produced simultaneously with the IVUS examination and the information they must depict with detail is the lumen and not the catheter itself. Perpendicular projections are desirable because of the amount of the spatial information they contain, but it is not a prerequisite, since the method can easily be extended to produce a three-dimensional model processing two angiographic images with known projection angles.

IV. CONCLUSIONS

The study of the three dimensional geometry of atherosclerotic arterial segments is a challenging issue. Several imaging techniques provide useful information about the vessel, but the production of a reliable three-dimensional model requires the combination of data from different imaging techniques. We have developed a method that successfully combines

the information from IVUS and angiographic images. The image segmentation method, presented in this paper, includes automated detection of the region of interest in IVUS images and shows a good overall performance. The method needs an initial estimation of the regions of interest only for the first frame. The use of deformable models with modified energy function and convex hull computations ensures fast convergence in sequential frames. The use of angiographic images provides information about the vessel geometry in 3D space.

With the results obtained from the application of the proposed method (Fig. 13) we can extract quantitative and qualitative information for the distribution of the plaque and the severity of the disease. The morphology of the arterial wall, the stenotic segments and the curvature in 3D space is depicted in the reconstructed model, while it is feasible to make volumetric computations or eccentricity estimations on the extracted model.

ACKNOWLEDGMENT

This work is partially supported by the Greek General Secretariat for Research and Technology in the framework of the project "PENED 318- An intelligent System for the Early Diagnosis of Coronary Artery Disease". We are grateful to Prof. A. Likas for his suggestions and valuable comments.

References

[1] C. Pellot, I. Bloch, A. Herment, F. Sureda, " An attempt to 3D reconstruction vessel morphology from x-ray projections and intravascular ultrasounds modeling and fusion ", Computerized Medical Imaging and Graphics, **20**, No 3, 141, 151, 1996.

[2] G. P. M. Prause, S.C. DeJohn, C.R. McKay, M. Sonka, "Towards a geometrically correct 3-D reconstruction of tortuous coronary arteries based on biplane angiography and intravascular ultrasound", International Journal of Cardiac Imaging, **13**, 451-462, 1997.

[3] A. Wahle, G.P.M. Prause, S.C. DeJong, M. Sonka, "Accurate 3-D fusion of angiographic and intravascular ultrasound data", Computers Assisted Radiology and Surgery, 24-27, Tokio, June 1998.

[4] A. Wahle, G.P.M. Prause, S.C. DeJohn, M. Sonka, "Geometrically correct 3-D reconstruction of intravascular ultrasound images by fusion with biplane angiography-methods and validation", IEEE Transactions on Medical Imaging, **18**, No 8, 686-699, August 1999.

[5] M. Sonka, X. Zhang, M. Siebes, M.S. Bissing, S.C. DeJong, S.M. Collins, C.R. McKay, "Segmentation of intravascular ultrasound images: A knowledge-based approach", IEEE Transactions on Medical Imaging, **14**, No. 4, 719-732, December 1995.

[6] X. Zhang, C.R. McKay, M. Sonka, "Tissue Characterization in intravascular ultrasound images", IEEE Transactions on Medical Imaging, **17**, No. 6, December 1998.

[7] D. Gil, P. Radeva, J. Saludes, J. Mauri, "Automatic Segmentation of Artery wall in coronary IVUS images: A probabilistic Approach", Proceedings of CIC'2000 Cambridge, Massachusetts, September 2000.

[8] C. Haas, H. Ermet, S. Holt, P. Grewe, A. Machraoui, J. Barmeyer, "Segmentation of 3D Intravascular Ultrasonic images Based on a radom field model", Ultrasound in Medicine & Biology, **26**, No. 2, 297-306, 2000.

[9] G. Kovalski, R. Beyar, R. Shofti, H. Azhari, "Three-dimensional automatic quantitative analysis of intravascular ultrasound images", Ultrasound in Medicine & Biology, **26**, No. 4, 527-537, 2000.

[10] R. Shekhar, R.M. Cothren, D.G. Vince, S. Chandra, J.D. Thomas J. D., J.F. Cornhill, "Three-dimensional segmentation of luminal and adventitial borders in serial intravascular ultrasound images", Computerized Medical Imaging and Graphics, **23**, 299-309, 1999.

[11] P. Brathwaite, K. Chandran, D. McPherson, E. Dove, "3D IVUS Border Detection in Highly Diseased Arteries with Dissecting Flaps", Computers in Cardiology, **25**, 157-160, 1998.

[12] T. Hagenaars,E.J. Gussenhoven, J.A. Van Essen, J. Seelen, J. Honkoop, A. Van Der Lugt, "Reproducibility of volumetric quantification in intravascular ultrasound images", Ultrasound in Medicine & Biology, **26**, No. 3, 367-374, 2000.

[13] C. Von Birgelen, C.S. Mintz, A. Nicosia, D.P. Foley, W.J. Van Der Giessen, "Electrocardiogram-gated intravascular ultrasound image acquisition after coronary stent deployment facilitates on-line three dimensional reconstruction and automated lumen quantification", Journal of American College of Cardiology (JACC), **30**, No 2, 436-43, August 1997.

[14] A. Wahle, E. Wellnhofer, I. Mugaragu, H. Sauer, H. Oswald, E. Fleck, "Assesment of diffuse coronary artery disease by quantitative analysis of coronary morphology based upon 3-D reconstruction from biplane angiograms", IEEE Transactions on Medical Imaging, **14**, No 2, 686-699, August 1995.

[15] P. Windyga, M. Garreau, M. Shah, H. Breton, J. Coatrieux, "Three dimentional reconstruction of the coronary arteries using *a priori* knowledge", Medical & Biological Engineering & Computing, **36**, 158-199, March 1998.

[16] K. Rosenfield, D.W. Losordo, K. Ramaswamy, J.O. Pastore, R.E. Langevin, S. Razvi, B. D. Kosowsky, J. M. Isner, "Three-dimensional Reconstruction of human coronary and peripheral arteries from images recorded during two-dimensional intravascular ultrasound examination", Circulation, **84**, No 5, 1938-1956, November 1991.

[17] J.C.H. Schuurbiers, C. Von Birgelen, J.J. Wentzel, N. Bom, P.W. Serruys, P.J. De Feyter, C.J. Slager, "On the IVUS plaque volume error in coronary arteries when neglecting curvature", Ultrasound in Medicine & Biology, 26, No 9, 1403-1411, 2000.

[18] K.R. Subramanian, M.J. Thubrikar, B. Fowle, M.T. Mostafavi, M.W. Funk, "Accurate 3D reconstruction of complex blood vessel geometries from intravascular ultrasound images: in vitro study", Journal of Medical Engineering & Technology, **24**, No 4, 131-140, July/August 2000.

[19] M. Kass, A. Witkin, D. Terzopoulos, "Snakes: Active contour models", International Journal of Computer Vision **1**, 321-331. 1987.

[20] J.J. Hopfield, "Neurons with graded response have collective computational properties like those of two-state neurons", Proc. Natl. Acad. Sci. USA, **81**, 3088-3092, May 1984.

[21] Y. Zhu, H. Yan, "Computerized tumor boundary detection using a hopfield neural network", IEEE Transactions on Medical Imaging, **16**, no 1, February 1997.

[22] F.P. Preparata, M.I. Shamos, "Computational Geometry, An Introduction", Springer-Verlag, 1998.

Figure Captions

Figure 1: Initial Estimation of the Region of Interest

Figure 2: Neural Network Architecture

Figure 3: Image Gradient Computation at a Specific Pixel of the Image

Figure 4: Extraction of the Media/Adventitia Boundary using (a) the Proposed Image Energy in Sequential Frames and (b) a Conventional Gradient Operator for the expression of image energy.

Figure 5: Extraction of the Media/Adventitia Boundary (a) using the Computation of the Convex Hull in Sequential Frames and (b) without the Computation of the Convex Hull.

Figure 6: Final Boundary Estimation Based on the Computation of the Convex Hull.

Figure 7: The Detected Boundaries for the Lumen and Media/Adventitia Borders.

Figure 8: Catheter's Path Extraction in 3D Space using two Perpendicular Angiographic Images.

Figure 9: Lumen's Centerline Computation.

Figure 10: Placement of each Frame along the Catheter's Path Through the use of a New Orthogonal Coordinate System.

Figure 11: Different Directions of the Vector Product Depending on the Turn of the Three Sequential Points.

Figure 12: Three – Dimensional Grid Visualisation of the Lumen.

Figure 13: (a) Three – Dimensional Grid Visualisation of the Lumen and the Outer Border of the Vessel, and (b) Three – Dimensional Solid Visualisation of the same Structures.

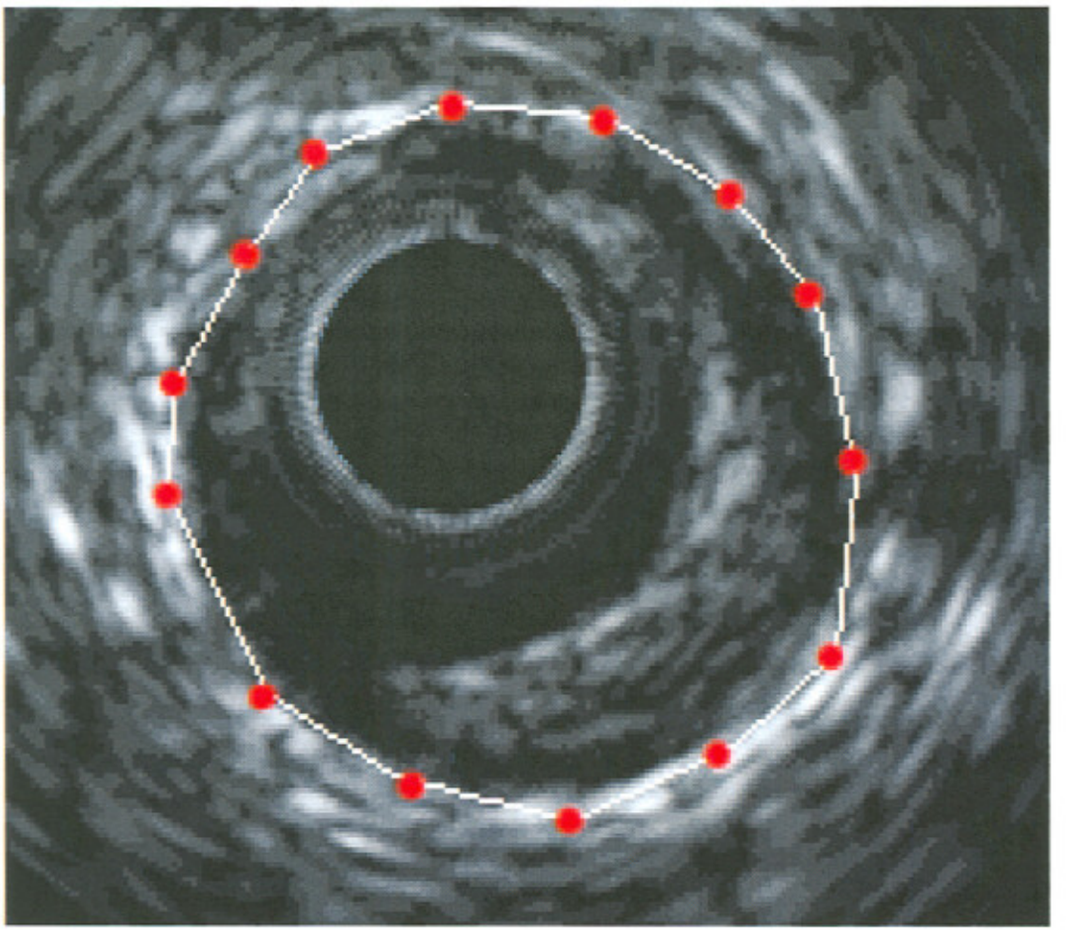

FIG 1

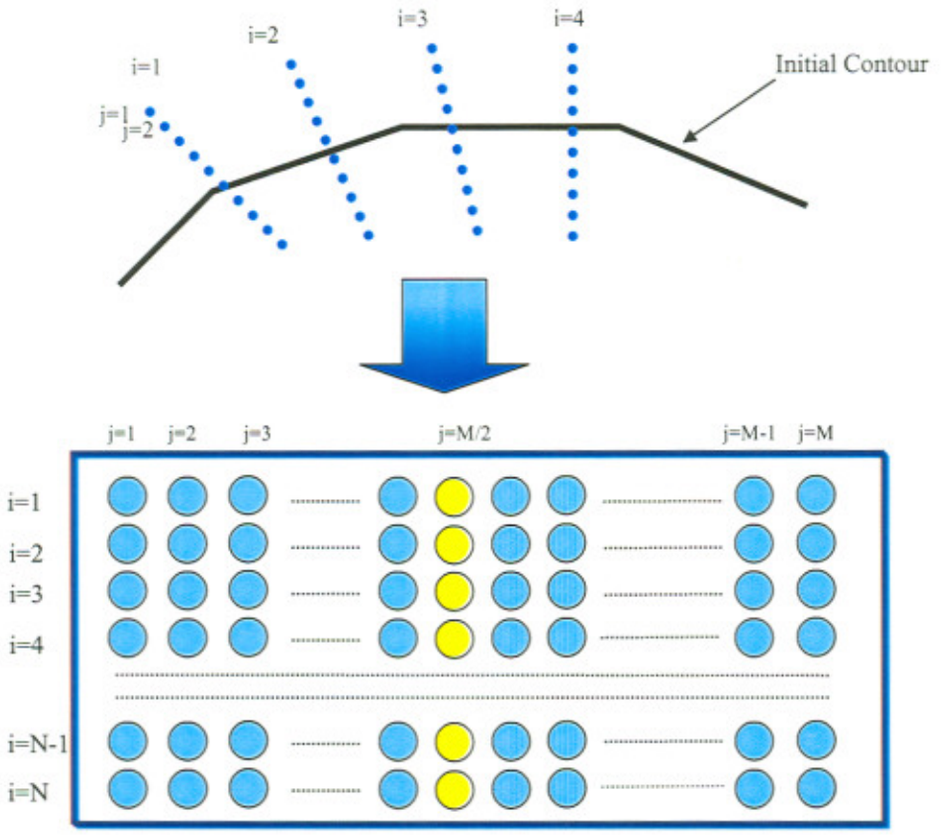
i=1
i=2
i=3
i=4
Initial Contour
j=1
j=2
j=1
j=2
j=3
j=M/2
j=M-1
j=M
i=1
i=2
i=3
i=4
i=N-1
i=N

F1G 2

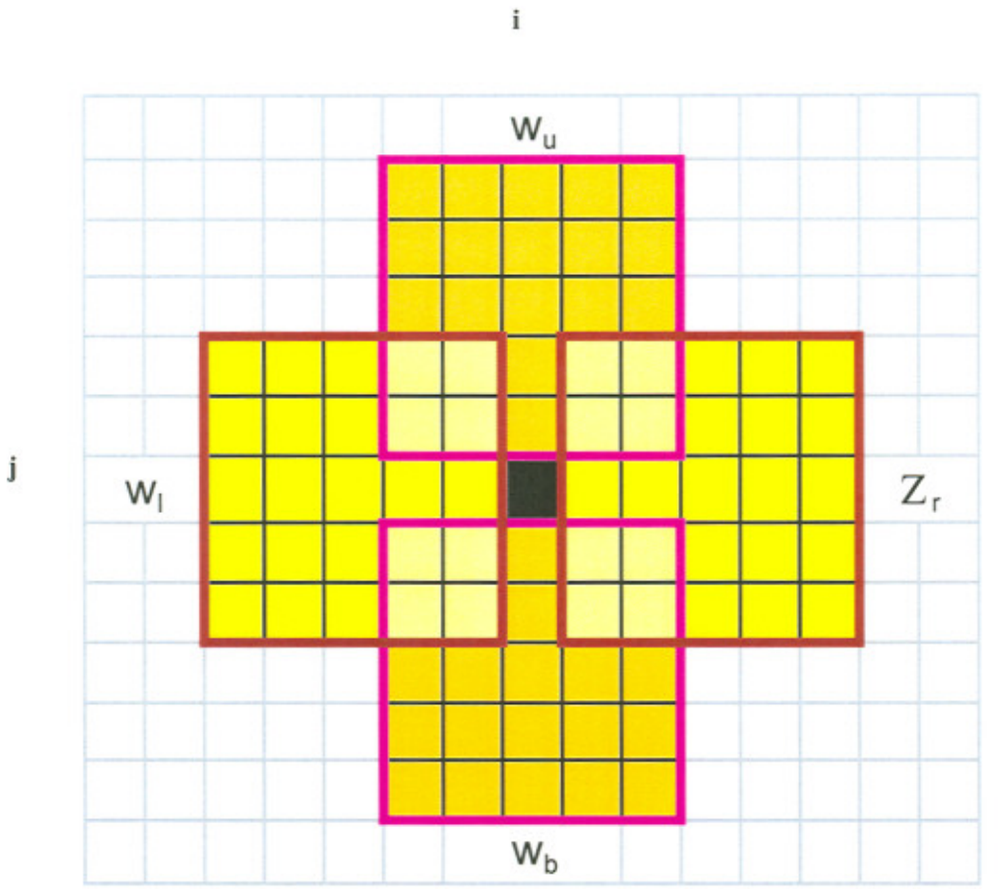

FIG 3


Not for diagnosis
16:04:40 0034
Not for diagnosis
16:04:40 0035
Not for diagnosis
16:04:40 0036

(a)


Not for diagnosis
16:04:40 0034
Not for diagnosis
16:04:40 0035
Not for diagnosis
16:04:40 0036

(b)

FIG 4

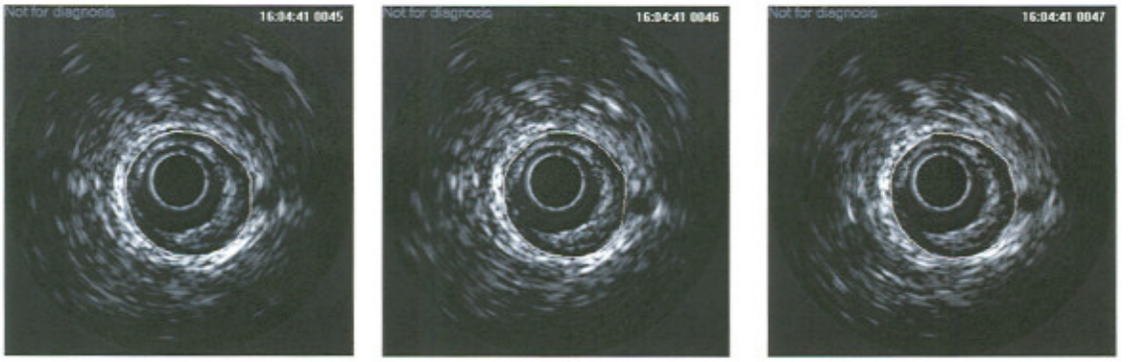
Not for diagnosis
16:04:41 0045
Not for diagnosis
16:04:41 0046
Not for diagnosis
16:04:41 0047

(a)


Not for diagnosis
16:04:41 0045
Not for diagnosis
16:04:41 0046
Not for diagnosis
16:04:41 0047

(b)

FIG 5

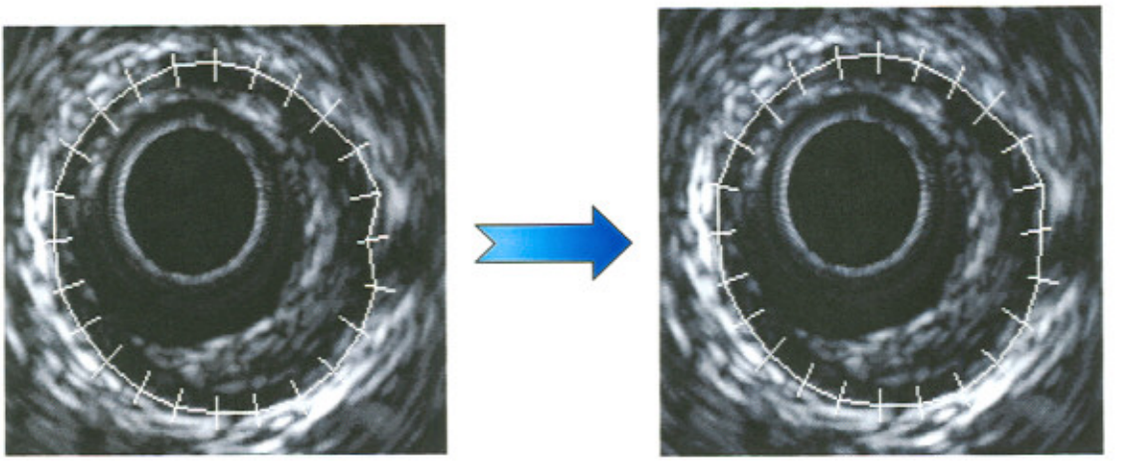

FIG 6

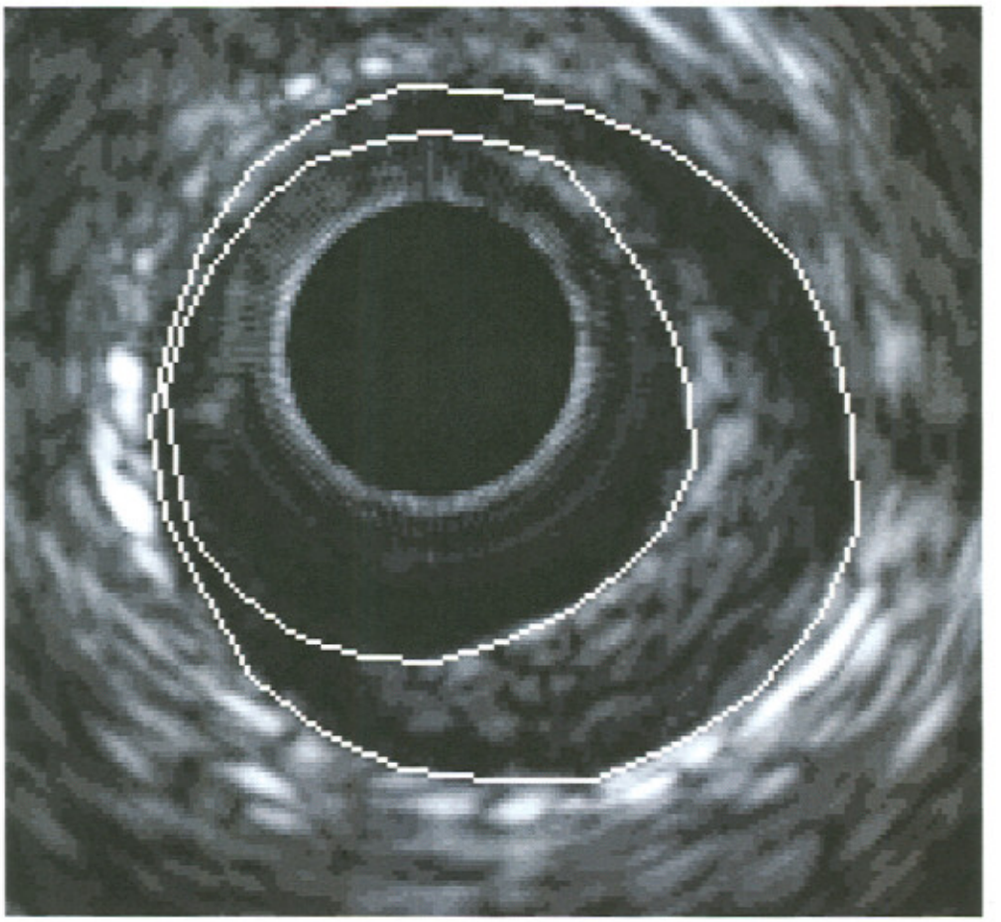

FIG 7

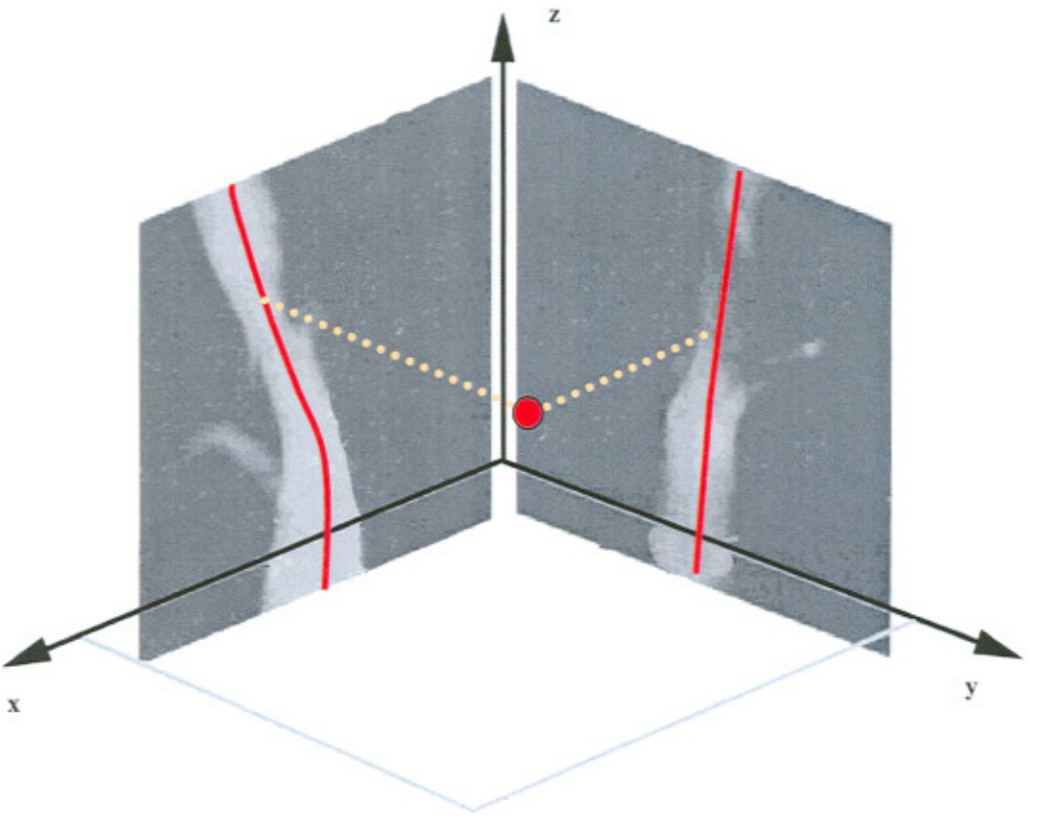

FIG 8

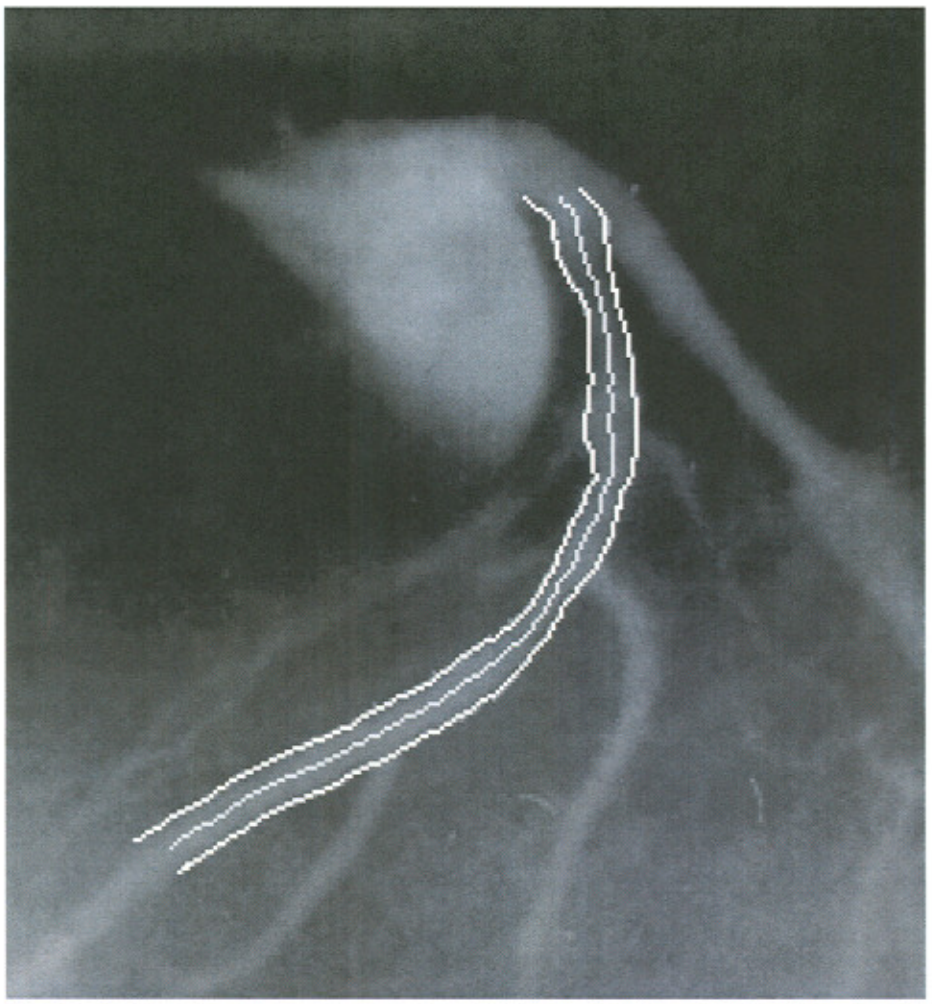

FIG 9

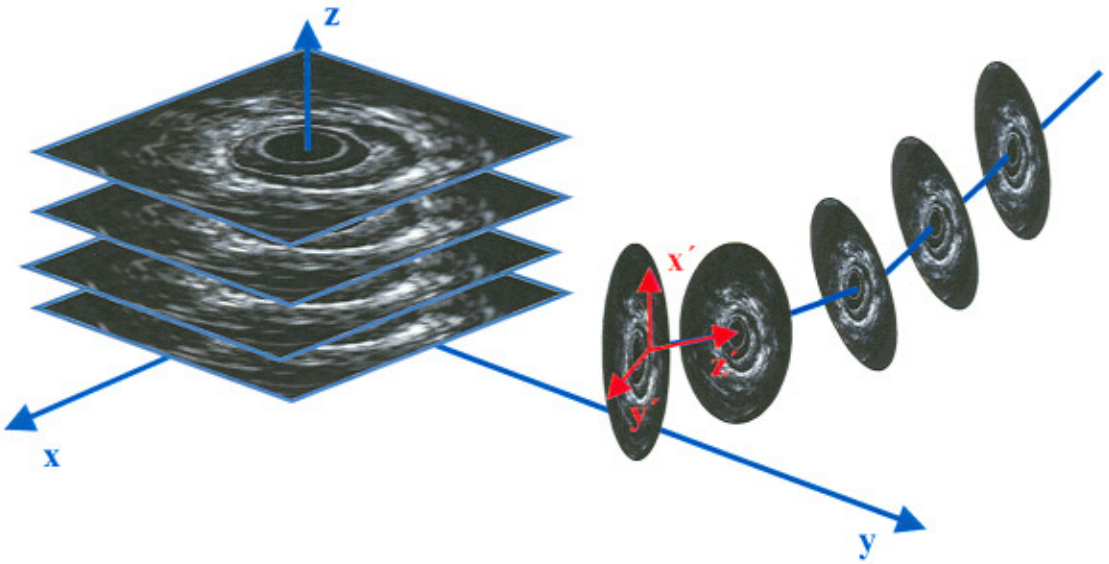

FIG 10

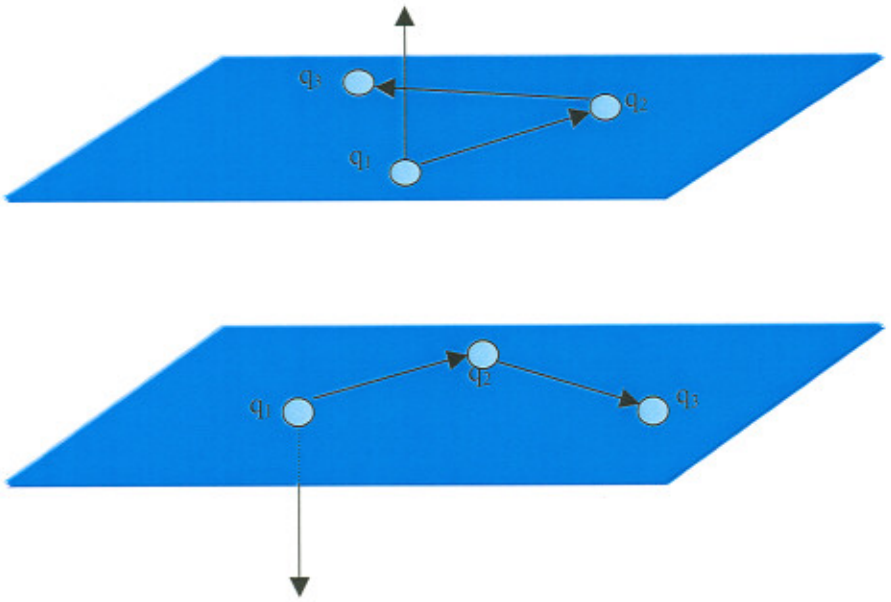

FIG 11

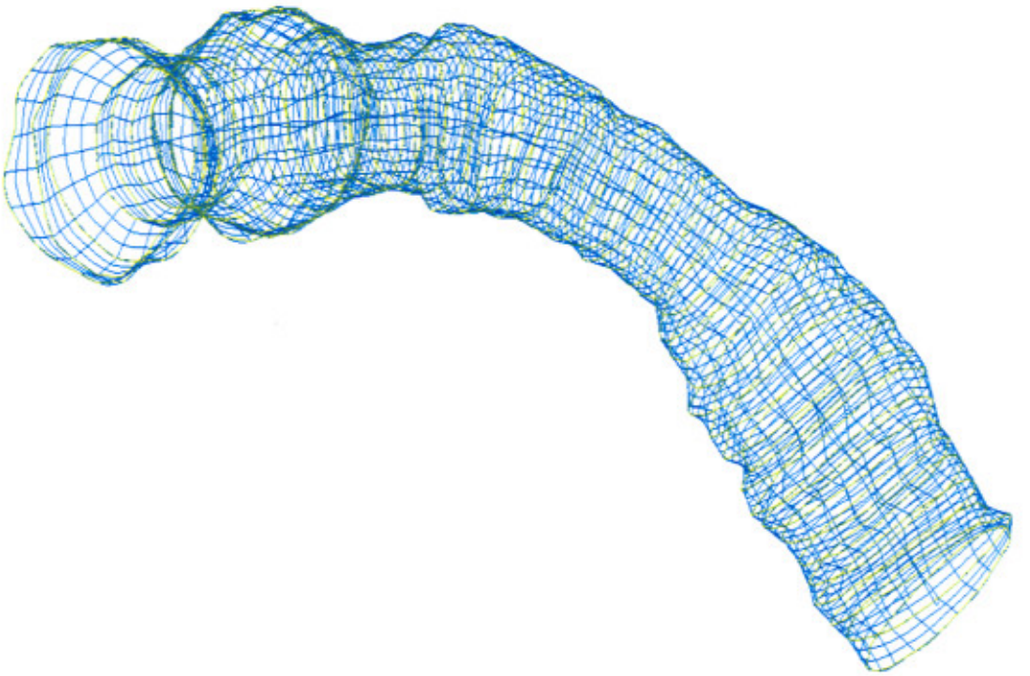

FIG 12

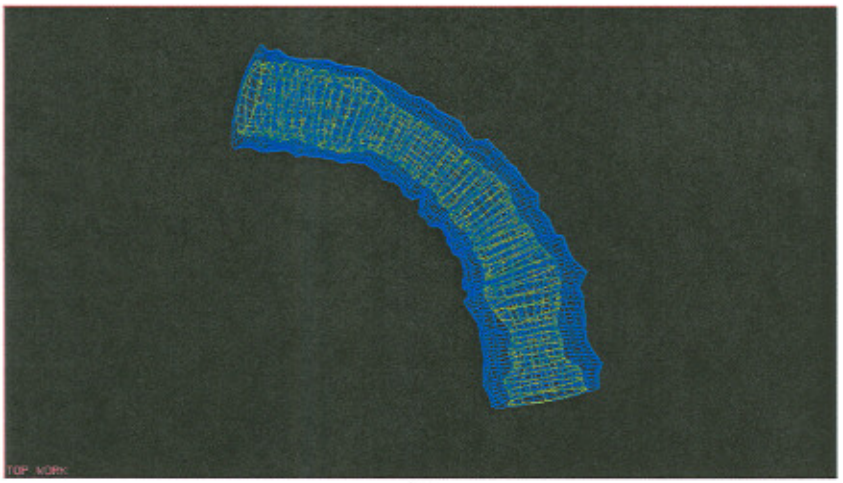

(a)

(b)

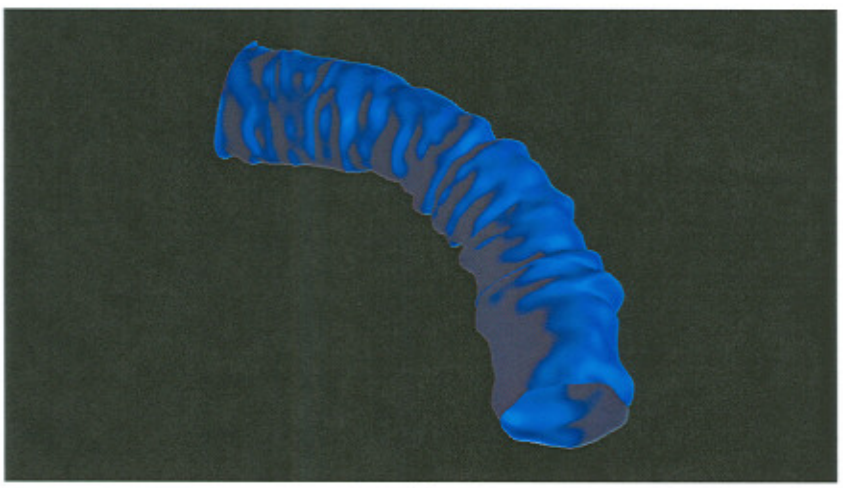

(c)

FIG 13